effect and various hypotheses on their origin have been made.[10,11] Though the states detected in the present work depend on surface treatment, presently available information does not allow a definite conclusion as to their nature. Nevertheless, a few considerations follow directly from the experimental results: The spectrum of Fig. 1 does not show any evidence of transitions of type (i). For example, one would expect a signal, in phase with the field, caused by transitions from the valence band to the level responsible for peak $\beta$, at energies around 0.37 eV. The absence of such a transition suggests that this level has a wave function of $p$-type symmetry which allows transitions to the states of the conduction band near $\mathbf{k}=0$ ($s$ type) but not to those of the valence band ($p$ type at $\mathbf{k}=0$). On the other hand, the fact that peak $\beta$ is extremely narrow seems to suggest that only states of the conduction band very near $\mathbf{k}=0$ can be reached optically from the surface levels.

[10] G. Dorda, Czech. J. Phys. **13**, 272 (1963).
[11] Y. F. Novotozky-Vlasov and A. V. Rzhanov, Surface Sci. **2**, 93 (1964).

PHYSICAL REVIEW VOLUME 144, NUMBER 2 15 APRIL 1966

# Theory and Observation of Intrinsic Surface States on Ionic Crystals

JULES D. LEVINE AND PETER MARK
*RCA Laboratories, Princeton, New Jersey*
(Received 8 October 1965)

A comprehensive theory of surface states on ionic crystals has been derived using Seitz's approach to bulk crystal energy states as a starting point. Surface ions are considered equivalent to bulk ions except for their reduced Madelung constant. The relationship of surface levels to bulk bandgap is expressed as a function of surface geometry and bulk material properties, and it is calculated using classical electrostatics for many surfaces of 46 halides, oxides, and sulfides. Symmetry arguments show that only for a checkerboard-like surface are the surface states symmetrically disposed about midgap. Numerical calculations show that one electron trap is formed from each surface cation and one hole trap for each surface anion; trap depths should be deepest for HgS, CdS, and ZnS; and for a $(11\bar{2}0)$ CdS surface the trap depths should be 0.2 to 0.4 eV, depending on the effective ionic charge assumed of 0.5 to 2.0. Intrinsic surface states were detected on the $(11\bar{2}0)$ surfaces of vapor phase grown insulating CdS single crystal platelets. Photoconductivity experiments (response time and thermally stimulated currents) indicate that these surface states function as traps for the photocarriers (electrons and holes) from the bulk.

## I. INTRODUCTION

INTRINSIC surface states have been carefully investigated in the literature for metallic and covalent crystals,[1–11] but surprisingly not for ionic crystals. There are, at present, only rough and qualitative theoretical criteria for predicting the nature of intrinsic ionic surface states and the experimental conditions necessary for their observation.[12–14] Recently, evidence has accumulated pointing towards the detection of intrinsic surface states on CdS.[15–18]

It is desirable, therefore, to formulate theoretical guide lines for predicting intrinsic-surface-state behavior for all ionic crystals and their crystal faces, to state the experimental criteria to be met in observing these states, and to report, in some detail, the intrinsic-surface-state properties inferred from CdS crystals.

Surface-state calculations for metallic and covalent crystals have been based essentially on either of two models. In the Tamm model, one assumes that the crystalline potential function is monotonic (all poles positive) and periodic, terminating at the surface plane. Surface states in the Tamm model are characterized by Bloch wave functions damped normal to the surface plane. In the tight binding model, the lattice is considered to be a collection of weakly coupled atoms filling half space. Surface states in this model are bulk states slightly modified due to the surface asymmetry. Other hybrid surface-state models have also been proposed. These models cannot be used for the ionic crystal because of two features. First, the monotonic

[1] I. Tamm, Physik Z. Sowjetunion **1**, 733 (1932).
[2] W. Shockley, Phys. Rev. **56**, 317 (1939).
[3] E. T. Goodwin, Proc. Cambridge Phil. Soc. **35**, 205 (1939); **35**, 221 (1939); **35**, 232 (1939).
[4] J. Bardeen, Phys. Rev. **71**, 717 (1947).
[5] T. A. Hoffmann and A. Konya, J. Chem. Phys. **16**, 1172 (1948).
[6] J. Koutecky and M. Tomasek, J. Phys. Chem. Solids **14**, 241 (1960).
[7] T. B. Grimley, J. Phys. Chem. Solids **14**, 227 (1960).
[8] M. D. Glinchuk and M. F. Deigen, Fiz. Tverd. Tela **5**, 405 (1963) [English transl.: Soviet Phys.—Solid State **5**, 295 (1963)].
[9] J. Koutecky, J. Surface Sci. **1**, 280 (1964).
[10] *Solid Surfaces*, edited by H. C. Gatos (North-Holland Publishing Company, Amsterdam, 1964).
[11] V. Heine, Phys. Rev. **138**, A1689 (1965).
[12] N. F. Mott and R. A. Gurney *Electronic Processes in Ionic Crystals* (Dover Publications, Inc., New York, 1964), p. 86.
[13] P. P. Ewald and H. Juretschke, in *Structure and Properties of Solid Surfaces*, edited by R. Gomer and C. S. Smith (University of Chicago Press, Chicago, Illinois, 1953), p. 82.
[14] M. F. Deigen and M. D. Glinchuk, J. Surface Sci. **3**, 243 (1965).
[15] P. Mark, J. Phys. Chem. Solids **25**, 911 (1964).
[16] P. Mark, J. Phys. Chem. Solids **26**, 959 (1965).
[17] P. Mark, Trans. N. Y. Acad. Sci. **27**, 946 (1965).
[18] P. Mark, J. Phys. Chem. Solids **26**, 1767 (1965).

potential function of the Tamm model cannot apply to ionic crystals where the potential function has alternate positive and negative poles located at cation and anion sites. Second, the tight-binding approximation is invalid for ionic crystals because of the exceedingly long-range and low-convergence properties of the Coulomb potential.

The model to be followed here is different from those above. It is a simple extension of the classical model introduced by Seitz,[19] and Mott and Gurney[12] for treating ionic crystals. Surface ions will be distinguished from bulk ions only in their reduced Madelung constant. This electrostatic model is idealized and approximate, but serves the purpose of qualitatively and quantitatively categorizing the whole spectrum of all ionic crystals and all their crystal faces. Such a categorization has not proved possible for metallic or covalent crystals. Band broadening, surface rearrangement,[20] and fractional ionic charge subtleties will be considered after the purely classical model is presented. The main numerical results will be in the form of ratios of various surface and bulk properties; the ratios are expected to be more accurate than differences between absolute magnitudes. Predictions are made for 46 ionic crystals, for 8 crystal faces, and for arbitrary effective ionic charge.

Intrinsic surface states substantiating the theoretical predictions were observed on the $(11\bar{2}0)$ surface of insulating, photoconducting CdS crystals during the course of an investigation of photoinduced chemisorption on the surfaces of these crystals.[15–18] The experiments revealed that photogenerated electrons (majority carriers) from the bulk could become localized on the surface either by the formation of chemisorbed ions [e.g., $O_2+e\rightarrow O_2^-$] or in surface traps [e.g., $(\text{trap})+e\rightarrow(\text{trap})^-$] when the surface was free of chemisorbed ions.[16,17] It will be shown that these electron traps on the adsorbate-free surface exhibit many of the characteristics of intrinsic surface states and that there is no electrostatic limitation[21] to the filling of these traps with the type of CdS crystals used in this investigation.

## II. THEORY

### A. Bulk Band Structure

Consider an ionic crystal of the form $M_nX_m$, where $M$ is a metallic cation and $X$ is a nonmetallic anion. In the bulk crystal, anions interact to form the usual valence band; this is narrow and is fully occupied at 0°K. Also, cations interact to form the usual conduction band; this is broader and unoccupied at 0°K. In the discussion to follow, the valence and conduction bands will be idealized as discrete levels, and the percentage of ionic character will be idealized as 100%. Departures from these idealizations will be considered later.

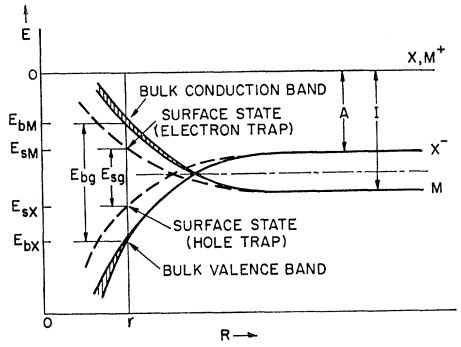


FIG. 1. Energy levels as a function of interionic distance $R$ for an ionic crystal $M_nX_m$. At the equilibrium distance $r$, the stable configuration is ionic due to the Madelung stabilization energy. Because surface ions have a reduced Madelung energy their energy levels are separated from those of the bulk.

The calculation of the bandgap and the valence- and conduction-band energies of ionic crystals can be easily carried out using the method of Seitz.[19] There are essentially two steps in the calculation. First, remove a test electron from the anion to outside the crystal; this energy input is the electron affinity $A$ plus the Madelung potential of the bulk anion $V_{bX}$. Second, bring the electron from outside the crystal to a distant cation site; this energy input is the Madlung potential of the bulk cation $V_{bM}$ minus the ionization potential $I$. The energies $A$ and $I$ refer to isolated atomic states. Let a mean Madelung bulk potential $V_b$ be introduced and defined as

$$V_b=\tfrac{1}{2}(V_{bX}+V_{bM}). \tag{1}$$

It follows from the above sequence that the bulk bandgap $E_{bg}$ is given by

$$E_{bg}=2V_b-(I-A). \tag{2}$$

To show how the bulk band states originate from the separated atomic states, consider an $M_nX_m$ crystal, shown in Fig. 1. This type of diagram has been used by Seitz[19] to describe electronic levels in alkali halides, ZnS and ZnO. The two electronic energy levels $M$ and $X^-$ are schematically indicated as functions of the interionic distance $R$. These levels are referred to a zero of potential associated with $M^+$ and $X$. In the limit of $R\rightarrow\infty$, the lower state is $M$, indicating that the system is most stable as isolated $M$ and $X$ atoms. As $R$ is decreased, the Madelung potential causes the $M$ and $X$ levels to become inverted so that the $X^-$ level falls below the $M$ level and the system prefers the ionic state consisting of $M^+$ and $X^-$ ions. The conduction tion state arises from the $M$ interactions. A suggestion of band formation is given by the shading in the figure.

The bulk conduction-band level $E_{bM}$ (formed from cations) and the bulk valence-band level $E_{bX}$ (formed

[19] F. Seitz, *The Modern Theory of Solids* (McGraw-Hill Book Company, Inc., New York, 1940), p. 408 ff., p. 447 ff.
[20] M. F. Tosi, Solid State Phys. **16**, 1 (1964).
[21] P. B. Weisz, J. Chem. Phys. **20**, 1483 (1952); **21**, 1531 (1953).

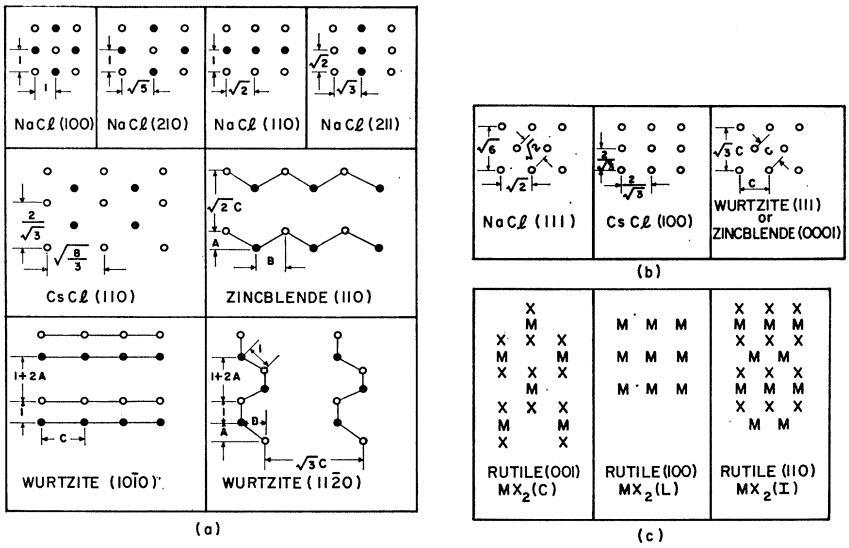


FIG. 2. Configurations of selected crystal surfaces: (a) surfaces of the class $MX(C)$; (b) surfaces of the class $MX(L)$; (c) surfaces of an $MX_2$ crystal. For the zinc-blende and wurtzite structures the parameters $A$, $B$, and $C$ are related to the tetrahedral angle 109.5°. They are $A=\sin 19.5°=0.334$, $B=\cos 19.5°=0.943$, and $C=(2+2A)^{1/2}=1.63$. The nearest interionic distance is taken as unity throughout.

from anions) are given by[19]

$$E_{bM}=V_{bM}-I\,, \tag{3a}$$

$$E_{bX}=-V_{bX}-A\,. \tag{3b}$$

The difference of these equations gives $E_{bg}$, and their arithmetic mean gives the bulk Fermi level. The effect of increasing the Madelung potentials $V_{bM}$ and $V_{bX}$ are to raise the conduction-band level and to depress the valence-band level. For crystals in which $V_{bM}=V_{bX}$, the Madelung interaction raises the conduction band and depresses the valence band by an equal amount. Band separation proceeds symmetrically about a fixed midgap position equal to $-(I+A)/2$. For crystals in which $V_{bM}\neq V_{bX}$, an unsymmetric band separation occurs.

How this classical interpretation of band separation in the ionic crystal bulk can be applied to the ionic crystal surface will be described below.

### B. Qualitative Survey of Surface-State Behavior

For simplicity consider first those bulk ionic crystals with the most symmetry. These have the designation $MX$. A simple symmetry operation can exchange positions of $M$ and $X$ ions. Thus, $V_{bM}=V_{bX}$ and the bulk conduction band is raised and the valence band is lowered by the same amount due to the Madelung potential. Crystals of the general type $M_nX_m$ do not have this property of a symmetric Madelung potential influence.

Surfaces of the $MX$ bulk crystal fall into two categories. One of these has an equal number of anions and cations in the surface plane. The resulting surface pattern resembles a regular or distorted checkerboard and will be called an $MX(C)$ surface, standing for "$MX$ checkerboard" surface. The other surface type has either anions along or cations alone in the surface plane with alternating ionic layers below the plane, similar to a layer cake; it will be called an $MX(L)$ surface, standing for "$MX$ layer" surface. No other categories are possible provided the ions are considered as point charges. Some $MX(C)$ surfaces are shown in Fig. 2(a). They are topologically similar to each other and can be interconverted by stretching. Some $MX(L)$ surfaces are shown in Fig. 2(b) which are also topologically similar. But $MX(C)$ and $MX(L)$ surfaces are topologically dissimilar.

Let us treat the $MX(C)$ surface in more detail. This is a two-dimensional representation of the three-dimensional crystal, having both anions and cations in the surface plane. It will be shown that surface cations are usually electron traps and surface anions are usually hole traps. Each surface level may be broadened into a narrow distribution of states, but this effect is not important for the discussion to follow.

The energy gap between the surface levels $E_{sg}$ (bandgap between the surface bands) is then obtained simply by using the analogous procedures of the previous section. The analogous equations are

$$E_{sg}=2V_s-(I-A)\,, \tag{4}$$

$$V_s=\tfrac{1}{2}(V_{sM}+V_{sX})\,, \tag{5}$$

$$E_{sM}=+V_{sM}-I\,, \tag{6a}$$

$$E_{sX}=-V_{sX}-A\,, \tag{6b}$$

where $V_{sM}$ and $V_{sX}$ are the Madelung potentials of surface cation and surface anion, respectively; and where $E_{sM}$ and $E_{sX}$ are the surface cation (usually electron trap) level and the surface anion (usually hole trap) level, respectively. $I$ and $A$ are independent of bulk or surface properties. The positions of the surface

levels with respect to bulk bands are shown schematically in Fig. 1.

For the $MX(C)$ surface, $V_{sM}=V_{sX}$ so that the Madelung interaction causes the surface cation level to be raised and the surface anion level to be lowered by the same amount. Thus, the $MX(C)$ surface levels are located symmetrically with respect to the center of the bulk bandgap. The $V_{sM}=V_{sX}$ symmetry does not hold for checkerboard surfaces of ionic crystals other than $MX$; some of these are shown in Fig. 2c for an $MX_2$ crystal.

To study the $MX(C)$ system more systematically, it is convenient to introduce the following dimensionless ratios:

$$\epsilon=E_{sg}/E_{bg}=\text{energy gap ratio}, \tag{7a}$$

$$\gamma=V_s/V_b=\text{geometry ratio}, \tag{7b}$$

$$\mu=(I-A)/2V_b=\text{material ratio}. \tag{7c}$$

By combining these with Eqs. (2) and (4), the desired result is obtained:

$$\epsilon=(\gamma-\mu)/(1-\mu). \tag{8}$$

It will be shown later that the parameters $\epsilon$, $\gamma$, $\mu$ vary within the approximate ranges $0<\epsilon<1$, $\frac{1}{2}<\gamma<1$, $0<\mu<\frac{1}{2}$. These ranges can be shown to be equivalent to the following statements: (1) Surface states formed from $M$ ions lie above the Fermi level within the bulk forbidden gap and will serve as electron traps; and (2) surface states formed from $X$ ions lie symmetrically below the Fermi level and will serve as hole traps, as indicated in Fig. 1. For $\epsilon\lesssim 1$, the surface states lie very close to the bulk bands and will be probably washed out by bulk band broadening. On the other hand, for $\epsilon\gtrsim 0$, surface states will lie close to bulk midgap and they will probably be observable in spite of bulk band broadening.

$MX(L)$ surfaces are expected to be more reactive and unstable than $MX(C)$ surfaces for the following two reasons. First, there is only one type of ion on the $MX(L)$ surfaces, so that a large electrical double layer will be formed (electrical field $>10^8$ V/cm). Second, to achieve stability the atomic rearrangements and relaxations on an *initial* $MX(L)$ surface will probably be severe because the lateral electrostatic repulsions in the $MX(L)$ surface layer tend to produce puckering. This surface puckering should be comparatively negligible for the $MX(C)$ surface where there is lateral electrostatic neutrality.

Surfaces of the general $M_nX_m$ ionic crystal cannot be treated in as complete a manner as in the $MX$ crystal. There are certain surfaces which resemble the $MX(C)$ and $MX(L)$ surfaces, but there are also others falling into different categories. Consider the $MX_2$-rutile ($TiO_2$) structures, for example, shown in Fig. 2(c). The (001) face has the same stoichiometry $MX_2$ as the bulk; hence, it is the analog of an $MX(C)$ surface. In addition, the (100) surface consists of all $M$ ions, so it is the analog of an $MX(L)$ surface. But the (110) surface has the surface stoichiometry $MX$ which would have properties in between $MX(C)$ and $MX(L)$. The surface levels in all these examples are not located symmetrically about a midpoint in the bulk bandgap. This follows because $V_{bM}\neq V_{bX}$ and $V_{sM}\neq V_{sX}$ in Eqs. (3) and (6). Thus, the theoretical study of crystals other than $MX$ promises complications, not simplifications, and will not be considered further.

This completes the qualitative survey of ionic crystal surfaces and their surface-state properties. To make the survey more quantitative, the geometry parameter $\gamma$ and the material parameter $\mu$ will be evaluated in some detail below.

### C. Calculation of $\gamma$

The parameter $\gamma(=V_s/V_b)$ gives the ratio of surface-to-bulk Madelung potential. With certain simplifications it is possible to calculate $\gamma$ in a straightforward manner. These simplifications are: (1) the anion-cation distance remains unchanged up to the surface plane,[20] and (2) the ion-core repulsions and Van der Waals attractions are neglected.[20] It is possible to calculate $\gamma$ without these simplifications but the goal in this theoretical effort is to sketch in the broad outlines of ionic surface-state behavior, not to become sidetracked with second-order effects. These effects will tend to increase $\gamma$ and they will be discussed more completely at the end of this section.

With the above simplifications the surface and bulk Madelung potentials for $MX$ crystals are given by

$$V_s=c_s ze/r, \tag{9}$$

$$V_b=c_b ze/r, \tag{10}$$

where $c_s$ is the surface Madelung constant, $c_b$ is the bulk Madelung constant, $z$ is the valence (possibly fractional), $e$ is the absolute magnitude of the unit electronic charge, and $r$ is the anion-cation distance. Note that $e$ appears to the first power because $V_s$ and $V_b$ are potential energy quantities with dimensions of volts. The ratio of Eqs. (9) and (10) gives

$$\gamma=c_s/c_b \tag{11}$$

which is dependent only on surface geometry and justifies calling $\gamma$ a "geometry parameter."

The bulk Madelung constant can be calculated from the usual Coulomb sum

$$c_b=\sum_{i,j,k} q_{ijk}/R_{ijk}=\sum_{i,j,k} Q, \tag{12a}$$

where $q_{ijk}$ is $\pm 1$, depending on the sign of the ion located at index position $(i,j,k)$, and $R_{ijk}$ is the distance measured from (0,0,0) to $(i,j,k)$, expressed in terms of the nearest cation-anion distance. The point (0,0,0) is excluded from the sum. As one example of the summing procedure consider a NaCl crystal for which $c_b=(6/1$

$-12/\sqrt{2}+8/\sqrt{3}-6/\sqrt{4}+\cdots$). Values of $c_b$ for the NaCl, CsCl, zinc-blende, and wurtzite crystals are known to be 1.748, 1.763, 1.638, and 1.641, respectively.[22]

The surface Madelung constant $c_s$ is calculated by considering the lattice potential at a point ion located of the free surface of a three-dimensional crystal. It is obtained from the sum

$$c_s=\sum_{i\geq 0,j,k} Q. \tag{12b}$$

Here the index $i$ is taken normal to the surface plane $i=0$, and the $j$ and $k$ indices have projections in the surface plane. As an example consider the (100) face of NaCl for which $c_s=(5/1-8/\sqrt{2}+4/\sqrt{3}-5/\sqrt{4}+\cdots)$. The computational procedure in calculating such a poorly converging sum can be considerably simplified if $c_b$ and $c_s$ are written in expanded forms as

$$c_b=\sum_{i=0} Q+\sum_{i>0} Q+\sum_{i<0} Q=\sum_{i=0} Q+2\sum_{i>0} Q, \tag{13}$$

$$c_s=\sum_{i=0} Q+\sum_{i>0} Q=\tfrac{1}{2}c_b+\tfrac{1}{2}\sum_{i=0} Q, \tag{14}$$

where the summing indexes $j$, $k$ are implied just as in Eqs. (12a) and (12b).

The ratio $\gamma=c_s/c_b$ then becomes

$$\gamma=\tfrac{1}{2}+\tfrac{1}{2}c_b^{-1}\sum_{i=0} Q. \tag{15}$$

The problem of computing $\gamma$ is thus reduced to computing the Madelung constant for the desired two-dimensional surface plane (sum over $i=0$, $j$, $k$), since $c_b$ is known. Equation (15) is extremely useful for calculating $\gamma$ of all $MX(C)$ surfaces, especially complex ones such as wurtzite $(11\bar{2}0)$ or zinc blende (110) shown in Fig. 2(a). But it cannot be used to calculate $\gamma$ for $MX(L)$ surfaces because each successive layer (sum over $i=0$, $j$, $k$; sum over $i=1$, $j$, $k$, etc.) yields an alternating $\pm\infty$ contribution to $\gamma$.

Using Eq. (14), calculations for $MX(C)$ surfaces were performed by taking sufficient neighboring ions in ringed groups to assure convergence from one group to another. Selected $\gamma$ values are given in Table I. Note that $\gamma$ can vary in the range $\frac{1}{2}<\gamma<1$. More highly sophisticated methods for performing specalized summations are also available.[20] To obtain physical insight into the variation of $\gamma$ with different crystal faces, a simple correlation was investigated. Define $\rho$ as the number of oppositely charged nearest neighbors of a surface ion divided by that of a bulk ion. For example, $\rho$ for the NaCl (100) face is 5/6. Values of $\rho$ are listed beside values of $\gamma$ in Table I. For the limited information available it is found that

$$\gamma\approx\rho+0.1\pm0.15. \tag{16}$$

[22] F. Seitz, Ref. 19, p. 76 ff.

TABLE I. $\gamma$ values calculated for selected $MX(C)$ ionic crystal surfaces.

| Lattice type | Surface face | $\gamma$ | $\rho$ |
|---|---|---|---|
| NaCl | (100) | 0.96 | 5/6 |
| NaCl | (110) | 0.86 | 4/6 |
| NaCl | (211) | 0.60 | 3/6 |
| NaCl | (210) | (0.77) | 4/6 |
| CsCl | (110) | 0.90 | 6/8 |
| wurtzite | $(11\bar{2}0)$ | 0.88 | 3/4 |
| wurtzite | $(10\bar{1}0)$ | 0.79 | 3/4 |
| zincblende | (110) | (0.85) | 3/4 |

Although this correlation is not very good, it was used to estimate $\gamma$ for $MX(C)$ cases which have not been explicitly calculated. Such estimates are shown surrounded by parentheses in Table I. No attempt has been made to calculate $\gamma$ for $MX(L)$ surfaces.

Complications arise in the calculation of $\gamma$ for stepped structures, since $\gamma$ differs from site to site along the step plane up to the step edge. Also, $\gamma$ will be slightly less than unity for ions in the planes beneath an ideally flat surface plane so that there will be subsurface states as well as surface states. The complications will not be considered further here.

It suffices to say that $\gamma$ can be calculated from simple geometric principles for important low-index surfaces of ionic crystals. A little consideration shows that the purely electrostatic part of surface tension or surface energy is proportional to $(1-\gamma)$. Thus, the more stable surfaces are those with smaller $(1-\gamma)$ or highest $\gamma$. For example, the NaCl crystal cleaves in the (100) plane for which $\gamma$ is highest at 0.96. Any surface rearrangement due to interionic repulsions, or van der Waals attractions, or any other effect will undoubtedly tend to relax the surface strains, to make the surface more stable, and to increase $\gamma$. Thus, $\gamma$ values in Table I are probably lower limits; the upper limit is unity.

### D. Calculation of $\mu$

The calculation of $\epsilon$ is, in general, dependent both on the geometric ratio $\gamma$ and on the material ratio $\mu$ through Eq. (8). In the special case of very small $\mu$, however, $\epsilon$ is independent of $\mu$ and is equal to $\gamma$.

To calculate $\mu$ explicitly, Eqs. (7c) and (10) can be combined to give

$$\mu=r(I-A)/2c_bze=0.0347r(I-A)/c_bz. \tag{17}$$

The coefficient 0.0347 arises if $r$ is expressed in angstroms and $(I-A)$ is expresses in volts. This equation will now be used to assign $\mu$ values to 46 typical halide, oxide, and sulfide ionic crystals of the form $MX$. Note that the $\mu$ parameter is a bulk property, independent of the surface crystal face.

For the 20 aklali halides it is a good approximation to set $z=1$. Seventeen of these crystals have the NaCl (fcc) structure; the other three have the CsCl (bcc) structure. Values of $\mu$ for these crystals are compiled

TABLE II. $\mu$ values calculated for selected $MX$ halides, oxides, and sulfides.

| Crystal | Lattice | $\mu$ | Crystal | Lattice | $\mu$ | Crystal | Lattice | $\mu(1)$ | $\mu(2)$ |
|---|---|---|---|---|---|---|---|---|---|
| LiF | NaCl | 0.04 | LiI | NaCl | 0.12 | BeO | Wurtz. | 0.25 | 0.47 |
| NaF | NaCl | 0.04 | NaI | NaCl | 0.11 | MgO | NaCl | 0.23 | 0.50 |
| KF | NaCl | 0.03 | KI | NaCl | 0.06 | CaO | NaCl | 0.19 | 0.50 |
| RbF | NaCl | −0.01 | RbI | NaCl | 0.05 | SrO | NaCl | 0.17 | 0.51 |
| CsF | NaCl | −0.02 | CsI | CsCl | 0.03 | BaO | NaCl | 0.16 | 0.52 |
| LiCl | NaCl | 0.07 | AgF | NaCl | 0.16 | BeS | Wurtz. | 0.36 | 0.51 |
| NaCl | NaCl | 0.06 | AgCl | NaCl | 0.21 | MgS | NaCl | 0.33 | 0.52 |
| KCl | NaCl | 0.02 | AgBr | NaCl | 0.21 | CaS | NaCl | 0.29 | 0.48 |
| RbCl | NaCl | 0.01 | AgI | Zinc bl. | 0.28 | SrS | NaCl | 0.26 | 0.47 |
| CsCl | CsCl | −0.01 | | | | BaS | NaCl | 0.25 | 0.48 |
| | | | CuCl | Zinc bl. | 0.18 | | | | |
| LiBr | NaCl | 0.09 | CuBr | Zinc bl. | 0.20 | ZnO | Wurtz. | 0.30 | 0.56 |
| NaBr | NaCl | 0.08 | CuI | Zinc bl. | 0.24 | ZnS | Zinc bl. | 0.41 | 0.57 |
| KBr | NaCl | 0.03 | | | | CdO | NaCl | 0.31 | 0.60 |
| RbBr | NaCl | 0.03 | TlCl | CsCl | 0.14 | CdS | Wurtz. | 0.41 | 0.58 |
| CsBr | CsCl | 0.01 | TlBr | CsCl | 0.15 | HgS | Zinc bl. | 0.47 | 0.64 |
| | | | | | | PbS | NaCl | 0.37 | 0.60 |
| | | | | | | NiO | NaCl | 0.23 | 0.57 |

in Table II, using known ionization potentials,[23] anion-cation distances,[23] and electron affinities.[19] In general, $\mu$ increases with decreasing electronegativity difference. In three exceptional cases (RbF, CsF, and CsCl) $\mu$ is negative, because for these crystals $I<A$. The most significant observation from the table is the small absolute magnitude of $\mu$, i.e., $|\mu|<0.12$. This has the consequence that $\epsilon\approx\gamma$ to an excellent approximation for the alkali halides. This would still be true even if $z$ were, say, 0.8 instead of 1.0.

The nine silver, copper, and thallium halides present a more complex situation. Five of these crystals have the NaCl or CsCl typically ionic structures, but four have the zinc blende structure, capable of accepting considerable convalency in $sp^3$ tetrahedral bonding. For all these crystals we set $z=1$ in the absence of other information, realizing that it is only a fair approximation. Values of $\mu$ for these crystals, given in Table II, are uniformly greater than the alkali halides, the range being $0.15<\mu<0.28$. This is in agreement with the increase of $\mu$ with decreasing electronegativity difference noted for the alkali halides.

For the ten alkaline earth oxides and sulfides it is a poor approximation to assume 100% ionic character, so that the effective $z$ is definitely less than the ideal valence value of 2. Calculations of $\mu$ can proceed easily only if $z$ is an integer. As a result, valences $z=2$ and $z=1$ will both be considered in the calculations to follow, through the calculation for $z=1$ is probably more realistic than that for $z=2$.

If $z=1$ is chosen, than $I=I(1)$ and refers to the first ionization potential (i.e., $Ba\rightarrow Ba^+ + e$). Also $A=A(1)$ and refers to the first electron affinity (i.e., $S+e\rightarrow S^-$). For oxygen,[19] $A(1)$ is +2.2 V and for sulfur, $A(1)$ is estimated by Seitz[19] to be +1.2 V. Values of $\mu=\mu(1)$ are shown in Table II. The range is $0.16<\mu(1)<0.36$.

On the other hand, if $z=2$ is chosen, then $I=I(2)$ and refers to the second ionization potential (i.e., $Ba^+\rightarrow Ba^{++}+e$) and $A=A(2)$ refers to the second electron affinity (i.e., $S^-+e\rightarrow S^{--}$). For oxygen and sulfur $A(2)$ is estimated by Seitz[19] to be −9 and −5 V, respectively. Values of $\mu=\mu(2)$ are shown beside $\mu(1)$ in Table II. The range is $0.47<\mu(2)<0.52$. Note that $\mu(1)$ is always smaller than $\mu(2)$.

The $\mu$ value for nonintegral $z$ can be estimated from a linear extrapolation between $\mu(1)$ and $\mu(2)$.

For the zinc, cadmium, mercury, lead, and nickel oxides and sulfides it is also a poor approximation to assume $z=2$. The assumption $z=1$ is undoubtedly more accurate, although both $\mu(2)$ and $\mu(1)$ are compiled and shown in Table II. The range of $\mu(2)$ is $0.57<\mu(2)<0.64$ and of $\mu(1)$ is $0.23<\mu(1)<0.47$. Again, the preceding rule is followed that $\mu(1)<\mu(2)$ and that $\mu$ is greater, the smaller is the electronegativity difference. Of all the halides, oxides, and sulfides, the crystals with largest $\mu$ are the oxides and sulfides. In particular, the largest $\mu(1)$ is computed for HgS and the next largest $\mu(1)$ for CdS and ZnS. These crystals will have the smaller $\epsilon$. This means that their surface levels will lie relatively closer to the bulk midgap. They will be more prominent and less liable to be wiped out by valence- and conduction-band broadenings. In other words, if surface levels are to be observed at all, they will be observed more clearly in HgS, CdS, and ZnS. Surface states of the (100) NaCl crystal have their $\epsilon$ value closest to unity, so they will be least likely to be observed.

All these calculations of $\mu$ indicate that the effective $\mu$ is probably less than $\frac{1}{2}$. Coupled with the finding that that $\gamma>\frac{1}{2}$, it follows that $0<\epsilon<1$, as anticipated in Sec. IIB.

### E. Application to the $(11\bar{2}0)$ Face of CdS

Consider as a detailed numerical example the CdS crystal (wurtizite modification) for which surface-state

[23] *Handbook of Chemistry and Physics*, edited by C. D. Hodgman (Chemical Rubber Publishing Company, Cleveland, Ohio, 1961).

data will be reviewed in Sec. III. The particular surface experimentally investigated is $(11\bar{2}0)$. This is of the class $MX$(C) and it is shown in Fig. 2(a). It consists infinite zigzag chains (angle 109.5°) of alternating + and − ions lying in the surface plane. The chains are separated by about three interionic distances. Each surface ion has three nearest oppositely charged ions, whereas a bulk ion has four. From Table I it is seen that $\gamma=0.88$ for this $(11\bar{2}0)$ face.

To calculate $\mu$ for CdS it is necessary to first estimate the effective ionic charge $z$. This is a difficult problem. Values of $z$ have been estimated for an analogous compound ZnS by many workers and these values are reviewed by Birman.[24] From measurements of elastic, dielectric, and piezoelectric constants $z$ is estimated to be 0.3 (100% ionicity would give $z=2$); from the Reststrahl frequency and the dielectric constant, $z=0.51$: from hardness and cleavage studies, $z=0.7$; and from electronegativity considerations, $z=0.5$. Various theoretical papers give $z=1.7$ and $z=1.29$. Birman weighs all this evidence and concludes that $z$ is probably 0.5. If this value is accepted, then a linear extrapolation of the $\mu(2)$ and $\mu(1)$ values of Table II gives $\mu=\mu(0.5)=0.33$. Taking $\gamma=0.88$, one calculates from Eq. (8) that $\epsilon(0.5)=0.82$.

In terms of Fig. 1, the surface state labeled $M$ is formed from $Cd^{z+}$ ions, while the surface-state labeled $X$ is formed from $S^{z-}$ ions. The $Cd^{z+}$ state is unoccupied at 0°K and is an electron trap, not a donor. The $S^{-z}$ state is occupied at 0°K and is a hole trap, not an acceptor. There will be one trap for each surface ion. If the electron traps could be filled and the hole traps could be emptied so as to preserve electrostatic neutrality in the surface plane (trap inversion), a considerable quantity of trapped charge could be accommodated. For trap inversion concentrations approaching one per surface ion, the surface Madelung constant $c_s$ would be altered. This would perturb the trap levels and probably increase the evaporation rate.[25]

For $MX(C)$ surfaces the electron trap depth below the conduction band and the hole trap depth above the valence band are equal. Call this surface trap depth $E_{st}$. It is related to the bulk bandgap $E_{bg}$ by

$$E_{st}=(1-\epsilon)E_{bg}/2. \tag{18}$$

If we assume with Birman that $z\approx0.5$ and use the experimentally measured bandgap of 2.5 eV, then it follows that $E_{st}(0.5)=0.23$ eV. On the other hand, if $z$ were the ideal value of 2, and $E_{bg}$ were again taken as 2.5 eV, then $\epsilon(2)=0.72$ and $E_{st}(2)=0.35$ eV. The *experimentally measured* $E_{bg}$ is to be preferred over an *a priori* calculation of $E_{bg}$. In other words, the aim of this effort is to calculate the ratios or relationships of surface to bulk properties and then to use measured bulk properties as reference values. This procedure is inherently more accurate than calculating surface and bulk properties on an *a priori* basis. In summary, the above discussion shows that the surface traps on CdS $(11\bar{2}0)$ are expected to have energy depths in the range $0.2<E_{st}<0.4$ eV.

## III. EXPERIMENTAL

Measurements made to detect intrinsic surface states consisted of studying the behavior of the photocurrent flowing parallel to the large area surface of a CdS platelet crystal with this surface exposed to various ambients. The optical excitation was incident on the same surface. Since CdS is an $n$-type photoconductor, only the behavior of the photoelectrons are subject to direct observation; the behavior of the photo-holes can only be inferred indirectly from their influence on the electrons. The experiments showed that photoelectrons from the bulk could be localized on the surface in two types of "surface states"; either by the formation of chemisorbed ions when the surface is in contact with an acceptor adsorbate or in traps when no adsorbate is present. It is the purpose of this section to demonstrate experimentally that the surface electron traps of the adsorbate-free surface are intrinsic surface states. All the following equations are written in practical units.[26]

### A. Material Specifications

The measurements were performed with insulating ($\rho\approx10^{10}$ Ω cm at room temperature) and photoconducting CdS crystals prepared by growth from the vapor phase. They were in the form of platelets from 20 to 50 $\mu$ thick and had surface areas ranging from 0.05 to 0.02 cm$^2$. CdS has the wurtzite structure and a bandgap of 2.5 eV. The crystals grow naturally with their large surfaces parallel to the $(11\bar{2}0)$ plane as determined by x-ray analysis. This plane is normal to the $a$ axis and parallel to the optic $c$ axis. The surface states were detected on this surface which is of the class MX($C$).

Only those CdS crystals were used in which the optical excitation energy of greater-than-bandgap light migrates away from the illuminated surface by ambipolar diffusion of free carriers,[27] and which are rather insensitive photoconductors. Crystals with these properties were labeled class II in an earlier paper[15] to distinguish them from the very photosensitive crystals, labeled class I, which are not very suitable for these experiments. The reason for this is that the minority carrier (hole) lifetime $\tau_p$ of the class II crystals can be measured directly[17,27] and that these crystals tend to have larger $\tau_p$ values than the sensitive class I crys-

[24] J. L. Birman, Phys. Rev. **109**, 810 (1958).
[25] G. A. Somorjai and J. E. Lester, J. Chem. Phys. **43**, 1450 (1965).
[26] W. Shockley, *Electrons and Holes in Semiconductors* (D. Van Nostrand Company, Inc., Princeton, New Jersey, 1950), pp. 211–213.
[27] P. Mark, Phys. Rev. **137**, A203 (1965).

tals.[17,28] It will be shown later that the ability to observe high occupation of the intrinsic surface states depends critically on the magnitude of $\tau_p$.

The measurements were made with the natural surfaces of the crystals. Chemical etching (with HCl) had no reproducible effects on the results. Prior to each run, the crystal was heated to 150°C in a flowing dry atmosphere. This treatment led to reproducable measurements.[17]

The experimental arrangement for the measurements was described earlier.[16,17] Optical excitation was always with light of greater-than-bandgap energy.

### B. Experimental Complications from Chemisorbed Ions

Since the presence of chemisorbed ions interferes with the observation of the surface electron traps, it is instructive to review briefly the effects chemisorbed ions have on the surface.[17] The results of chemisorption experiments are consistent with a model that assumes that (1) the negative charge of the chemisorbed ions is compensated in an adjacent depletion layer by the positive space-charge of the photo-holes located in the recombination centers[16] (see energy band diagram of Fig. 3); (2) the diffusion of electrons and holes through the ensuing Schottky-type surface barrier dictates the chemisorption kinetics; and (3) the chemisorbed ions act as recombination centers for photocarriers; the steady-state photocurrent flowing parallel to the illuminated surface is always greater when this surface

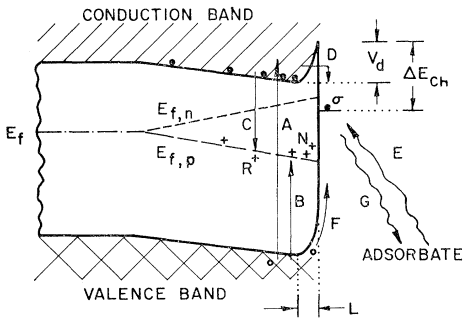


FIG. 3. Model for photo-induced chemisorption on the surface of an insulator. (A) Photo-excitation of free carriers; (B) rapid capture of photo-holes by the recombination centers $R$; (C) slower recombination transition; (D) and (E) chemisorption transitions; (F) and (G) photo-desorption transitions. Also shown are: the barrier thickness $L$ and the diffusion potential $V_d$; the energy depth $\Delta E_{ch}$ of the chemisorbed ions; the thermal equilibrium Fermi energy $E_f$; the steady-state quasi-Fermi energies of the photoelectrons and photo-holes $E_{f,n}$ and $E_{f,p}$, respectively; the surface ion concentration $\sigma$ and the compensating concentration $N_+$ of holes in the recombination centers in the depletion layer. The sloping of the bands represents the Dember field, the spatial extent of which is several ambipolar diffusion lengths. The Dember field is substantially constant because the conduction-electron concentration decreases exponentially with distance from the surface (see Ref. 27).

[28] A. Rose, Phys. Rev. **97**, 322 (1955); *Concepts in Photoconductivity and Allied Problems* (John Wiley & Sons, Inc., New York, 1963), Chap. 3.

is adsorbate-free than when there are chemisorbed ions on the surface.[16] This means that an appreciable fraction of the photo-holes reach the surface within the time interval $\tau_p$. The holes drift to the surface in the barrier field with the transit time

$$t_p = L^2/\mu_p V_d, \tag{19}$$

where $L$ is the barrier thickness, $V_d$ is the barrier diffusion potential, and $\mu_p$ is the hole mobility. If $t_p < \tau_p$ the chemisorbed ions can function as recombination centers. The ambipolar diffusion measurements[27] with the class II crystals show that $\tau_p \approx 30$ nsec, and the chemisorption measurements with the same crystals yield a value for $t_p$ in the neighborhood of 5 nsec.[16] Thus, the condition for desorption by minority carriers is fulfilled. If $t_p > \tau_p$, the chemisorbed ions would not act as recombination centers, and the surface would be able to accomodate more ions. The maximum concentration $\sigma_m$ of the surface charge, compensated in an adjacent depletion layer, is given by[17,21]

$$\sigma_m = (2K\epsilon_0 N_+ V_d/e)^{1/2} \text{ cm}^{-2}, \tag{20}$$

where $K$ is the dc dielectric constant (10 for CdS), $\epsilon_0$ is the electric permittivity of free space ($8.85\times10^{-14}$ F/cm), $N_+$ is the concentration ($\text{cm}^{-3}$) of positive species in the depletion layer which compensate the surface charge (in this case, it is the concentration of photo-holes in the bulk recombination centers), and $e$ is the magnitude of the electronic elementary charge ($1.6\times10^{-19}$ C). This formula is valid for any form of surface charge, whether or not it is in the form of chemisorbed ions, provided the surface charge is compensated in a depletion layer. For photoconducting CdS crystals, $\sigma_m$ cannot exceed $10^{11}$ $\text{cm}^{-2}$ or about $10^{-4}$ of the monolayer, and the maximum chemisorbed ion concentration is always less than about $5\times10^{10}$ $\text{cm}^{-2}$ because of minority carrier desorption.[16]

### C. Experimental Evidence for Surface Trapping

When $t_p < \tau_p$, the chemisorbed ions can be removed from the surface by photo-desorption.[15–18] This is accomplished by removing the adsorbate atmosphere, either by evacuation or by displacement with an inert gas (e.g., $N_2$ or the rare gases), while the surface is illuminated with light of greater-than-bandgap energy. When this is done, new surface states appear that function as traps for free carriers rather than as recombination centers.[16,17] This information is derived from the behavior of the photoconductivity response time and the thermally stimulated current, the magnitudes of which are closely related to the extent of carrier trapping.

The response time is the speed with which the photocurrent responds to a sudden change in the illumination level. It is equal to the electron lifetime $\tau_n$ in the absence of trapping and, to a first approximation, becomes larger than $\tau_n$ when traps are present by a factor equal to the

ratio of the trapped to free charge which is always greater than unity.[28] Experiments show that the response time of the class II crystals is as much as five decades longer when the surface is adsorbate-free than when it has an adsorbate (e.g., oxygen) chemisorbed on the surface.[15,16] The effect is illustrated by Fig. 4. Curves (a) and (b) show, respectively, the photoconductivity decay of a CdS crystal first with an adsorbate-free surface and then with chemisorbed oxygen on its surface. Curve (c) shows the sharp and rapid acceleration of the decay when oxygen is chemisorbed on the surface during the decay with an adsorbate-free

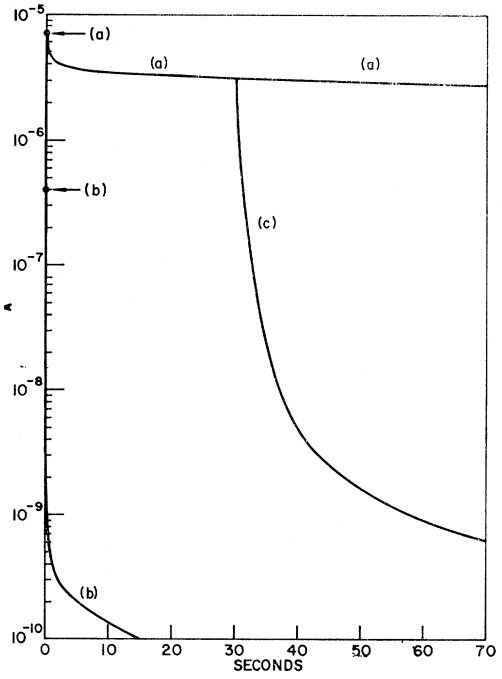


FIG. 4. Photoconductivity decay upon removal of excitation at room temperature. Curve (a): decay with an adsorbate-free surface measured in a nitrogen atmosphere after photodesorption in nitrogen; curve (b): decay in an oxygen atmosphere after photo-induced chemisorption of oxygen; curve (c): effect of admitting oxygen during the decay which commenced in nitrogen with an ion-free surface. Illumination flux density: $10^{14}$ photons/sec cm$^2$.

surface.[15] [*Note added in proof.* The sharp acceleration of the decay (curve (c)) on the admission of an adsorbate is the result of the interaction between the intrinsic surface states and the adsorbate. See P. Mark, RCA Rev. **26**, 461 (1965).]

The effects of the illumination intensity on the photoconductivity decay of a CdS class II crystal with chemisorbate-free surface is illustrated by Fig. 5. The response time (in this case, the time required for the photocurrent to decay by a factor of 2 when the illumination is switched off), is relatively fast, near the detectability of 5 msec set by the mechanical shutter, at low illumination and then becomes slower rather

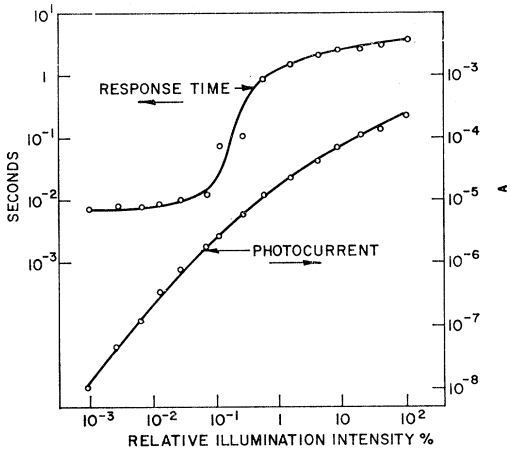


FIG. 5. Response time and photocurrent versus illumination level for an adsorbate-free surface. The response time is taken as the time required for the photocurrent to decay to one-half its steady-state value after sudden termination of the excitation. 100% intensity corresponds to a photon flux density of $3.5\times10^{16}$ photons/cm$^2$ sec. The intensity was varied with wire mesh filters.

abruptly by more than two decades as the illumination is increased. This behavior of the response time is accompanied by a sublinear dependence of the photocurrent on the illumination intensity.

Additional and independent evidence that trapping is strongly influenced by surface conditions is furnished by the behavior of the thermally stimulated current (abbreviated TSC). This is the current, in excess of the dark current, that is observed when a pre-excited photoconductor is heated in darkness to thermally release trapped carriers.[29] It is more quantitative measure of trapping than the response time. The number of trapped carriers release during the heating cycle is proportional to the area between the TSC and the dark current provided the heating rate is constant. The proportionality factor is the gain of the photoconductor.[28] The TSC measurements are consistent with the response time measurements; the TSC is several decades larger for an adsorbate-free surface relative to the TSC obtained with a chemisorbate (again oxygen) on the same surface.[16] The effect is illustrated by Fig. 6 where curves (a) and (b) are, respectively, the TSC for the adsorbate-free surface and the TSC with oxygen chemisorbed on the same surface. The corresponding dark currents are also shown. (The dependence of the dark current on surface conditions has been treated elsewhere.[16,18])

### D. Evaluation of the TSC Measurement

The number of trapped electrons $N_t$ released during the TSC measurement can be obtained from the relation

$$N_t = (1/e)\int_{\Delta T} (i_{\mathrm{TSC}}/Gh)\, dT. \qquad (21)$$

[29] R. H. Bube, *Photoconductivity of Solids* (John Wiley and Sons, Inc., New York, 1961), pp. 292–299.

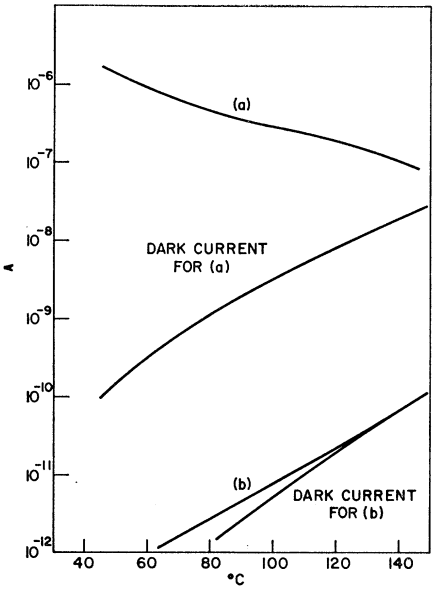


FIG. 6. Thermally stimulated current (TSC). Curve (a): TSC with an adsorbate-free surface measured in a nitrogen atmosphere after photodesorption in nitrogen; curve (b): TSC in an oxygen atmosphere after photo-induced chemisorption of oxygen. The corresponding dark currents are also shown. The heating rate for the TSC was 0.5°C/sec.

Here $i_{TSC}$ is the TSC; $h$ is the heating rate (0.5°C/sec); $T$ is the temperature in degrees centigrade; $\Delta T$ indicates the temperature interval of the TSC measurement; and $G$ is the gain of the photoconductor which is given by $G=(\tau_n/t_n)$ where $t_n$ is the inter-electrode transit time of the electrons. When the photoconductor is under illumination with the photon flux $I$, the gain is given by the relation[15]

$$G=i/eIS, \tag{22}$$

where $i$ is the photocurrent and $S$ is the illuminated surface area of the crystal provided the contacts are Ohmic and also illuminated. The light source used to obtain the data of Figs. 4 and 6 was a grating monochromator set at 0.45 $\mu$ and the photon flux incident on the crystal, as measured by a thermopile, was $10^{14}$ photons/sec cm$^2$. The exposed area was $8\times10^{-2}$ cm$^2$. For the adsorbate-free surface, the steady-state photocurrent under maximum illumination was 7 $\mu$A (see the $t=0$ current on Fig. 4) and the integrated area of the TSC curve is $4\times10^{-5}$ A°C. Inserting these numbers into Eq. (22), one obtains $G=5.5$ for maximum illumination and the evaluation of $N_t$ from Eq. (21) with this gain yields $N_t$ (adsorbate free)$=10^{14}$. Similarly, from the steady-state photocurrent with oxygen chemisorbed on the surface, one obtains $N_t$(oxygen) $=10^8$. Thus, there are apparently $10^6$ times as many electrons trapped when the surface is adsorbate-free than there are with oxygen chemisorbed on the surface.[30]

The rapid rate with which the response time changes during chemisorption [curve (c) of Fig. 4] excludes the possibility of diffusion of impurities into and/or from the bulk as a source of the adsorbate-dependent trapping. This would require an unrealistically large diffusion coefficient of $10^{-10}$ cm$^2$/sec at room temperature.[16] It is evident that the trapping effect observed with the adsorbate-free surfaces is a true surface phenomenon in the sense that the trapped electrons are situated in surface states. But then the released charge measurement of the TSC, when normalized to the surface area of the crystal ($8\times10^{-2}$ cm$^2$), would require that about $10^{15}$ electrons/cm$^2$ can be trapped on an adsorbate-free surface. Bube has also reported similar observations.[31] Thus, despite the fact that the electrons that occupy the surface traps originate in the adjacent bulk, one measures an apparent surface-trapped electron concentration about four decades in excess of what can be compensated in an adjacent depletion layer [Eq. (20), and that is approximately equal to the surface lattice site concentration.

### E. Interpretation of the Surface Traps as Intrinsic Surface States

To account for this apparently unusually large coverage by trapped carriers, the tentative suggestion was advanced[16,17] that the electrons trapped on the ion-free surface are not compensated in a depletion layer, but rather by a nearly equal number of holes that are also trapped on the surface, so that there is only a small *net* surface charge relative to the adjacent bulk. That is, the trapping is surface compensated. However, it is doubtful whether electrons and holes of concentrations approaching one per surface lattice site can be trapped on the surface without appreciable direct recombinations. The dilemma can be resolved by realizing that an electron released from a surface trap into the bulk during the photoconductivity decay or the TSC cannot recombine until a compensating hole is also released from its surface trap into the bulk.[32] The effect of this is that the lifetime in the conduction band of the electrons released from the surface traps can be much greater than the photoconductivity lifetime calculated from the photoconductivity gain [Eq. (22)]. The latter is the lifetime of the electrons excited from the valence band by optical transitions. Thus, using the photoconductivity lifetime in the gain to evaluate $N_t$ from the TSC would tend to give spurriously large values of $N_t$. Nevertheless, to affect the magnitude of the response time and of the TSC in this way, it is necessary to trap both electrons and holes on the surface in nearly equal numbers so that there must be surface states for both carrier types. This, together with the additional facts

[30] The remaining pertinent data for this crystal are: $d=0.2$ cm, $\mu_n\simeq200$ cm$^2$/V sec, and $V=10$ V. Thus, $t_r=20$ $\mu$sec. Also, $\tau_n$ can be obtained from Eq. (4) of Ref. 15 and turns out to be about 100 $\mu$sec, in good agreement with diffusion measurements (see Ref. 27).

[31] R. H. Bube, J. Appl. Phys. 34, 3309 (1963).

[32] We are indebted to M. A. Lampert for pointing this out to us.

that these surface states are traps and that they are observed only after desorption when no chemisorbate is present, is taken as an indication that they are intrinsic surface states.

The existence of the intrinsic surface states that function as traps for photocarriers of both signs allows the surface to accomodate electrons from the bulk so as to obviate the restriction set by Eq. (20). This process is envisioned as follows with the aid of the band diagrams shown on Fig. 7. The energy-band configuration near the surface in thermal equilibrium is shown in (a) for an adsorbate-free surface. The possible energy distribution of the surface traps as well as their occupation is schematically indicated. When the surface is illuminated with strongly absorbed light, electrons and holes are optically generated in the bulk. Since the material is an $n$-type photoconductor, the electron concentration $n$ in the conduction band exceeds the hole concentration $p$ in the valence band by several decades, reflecting the fact that $\tau_n \gg \tau_p$.[28] Charge neutrality is maintained in the bulk by the recombination centers which localize most of the photo-holes very rapidly. It is assumed that the bands are very nearly flat (i.e., no surface barrier) for the adsorbate-free surface just after illumination commences,[16] which is consistent with the theoretical development (Sec. IB), and that the capture cross sections of the surface traps for their respective carrier types are roughly the same. Thus, the initial probability per unit time for transitions of electrons into their surface traps is much greater than that for holes into their surface traps because $n \gg p$, and the electron traps fill more rapidly at the outset than the hole traps. At this stage, the electrons in the surface traps are compensated principally by the holes in the recombination centers in the adjacent bulk and a depletion-type Schottky barrier begins to form in analogy to the chemisorption process.[16] This is shown in (b).

What happens next depends critically on the magnitude of the minority carrier lifetime. The holes tend to drift to the surface in the barrier field with the transit time given by Eq. (19). If $\tau_p < t_p$, the holes will not reach the surface. The electrons in the surface traps will remain compensated in the depletion layer as shown in (b), and the filling of the traps cannot exceed the electrostatic limitation of Eq. (2); that is, occupation is limited to about $10^{-4}$ of a monolayer [$\sim 10^{10}-10^{11}$ cm$^{-2}$]. Thus, (b) illustrates the steady-state filling of surface traps when $\tau_p < t_p$. However, if $\tau_p > t_p$, holes will reach the surface and will become localized in the hole traps near the valence band. The negative charge of the occupied electron surface traps will now become compensated by the positive charge of the holes in the hole surface traps rather than by the holes in the recombination centers in the depletion layer and occupation of the electron traps can now exceed the electrostatic limitation. But there will always be a slight depletion-type barrier at the surface, the function of

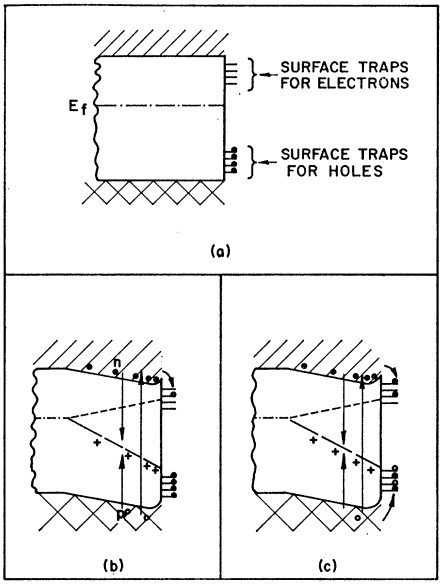


FIG. 7. Model for the surface traps of an adsorbate-free surface as deduced from the experiments. (a) Surface at thermal equilibrium showing two distinct sets of surface traps. The levels near the conduction band are unoccupied and serve as electron traps, while the states near the valence band are occupied and serve as traps for holes. (b) Surface just after illumination commences. The electron traps begin to fill and a smlll surface barrier appears. The hole traps are still essentially unoccupied by holes. This figure also describes the steady-state condition when $t_p > \tau_p$. (c) Steady-state condition under illumination when $t_p < \tau_p$. The electron and hole traps are now nearly equally occupied by electrons and holes, respectively.

which is to simultaneously retard the filling of the electron traps and to accelerate the filling of the hole traps so as to offset the discrepancy between $n$ and $p$. The steady-state surface configuration when $\tau_p > t_p$ is shown in (c).

The relative magnitudes of $\tau_p$ and $t_p$ also determine the behavior of the response time shown on Fig. 5; namely that the response time becomes slower with increasing illumination. It is worth emphasizing that this behavior is unusual. In a homogeneous photoconductor in which the response time is determined by trapping, there is no model involving transitions among bulk energy levels leading to a response time that increases with increasing illumination level.[28,33] However, the present model of surface trapping indicates the following explanation.

The relation between $L$, $V_d$, and $N_+$ in a Schottky-type barrier is given by[34]

$$L^2 = 2K\epsilon_0 V_d / eN_+ . \tag{23}$$

When this relation is combined with Eq. (19), one

[33] A. Rose, RCA Rev. 12, 362 (1951).

[34] For example, see A. van der Ziel, *Solid State Physicsl Electronics* (Prentice-Hall, Inc., Englewood Cliffs, New Jersey, 1957), pp. 241–253.

finds that

$$t_p = 2K\epsilon_0/e\mu_p N_+. \quad (24)$$

That is, the transit time of the holes through the barrier is inversely proportional to the positive space-charge concentration in the depletion layer. For a photoconductor, $N_+$ is the concentration of photo-holes in the recombination centers. If the photocurrent is proportional to the illumination level $I$ (photons/sec cm$^2$), $N_+$ is constant.[28] But if the photocurrent is sublinear; that is, if it increases less rapidly than in proportion to $I$, then $N_+$ must increase and, through Eq. (24), $t_p$ must decrease with increasing $I$.[28] Thus, the possibility exists that $t_p > \tau_p$ for small $I$ and that $t_p < \tau_p$ for large $I$ when the photocurrent-intensity dependence is sublinear.

The observation of this transition is illustrated by Fig. 5. At low $I$ the response time is short and characteristic of the situation of few traps. In this region $t_p > \tau_p$; the occupation of the electron surface traps is held down because the holes cannot reach their surface traps. As $I$ is raised, $t_p$ becomes smaller because the photocurrent is sublinear. When the condition $t_p \approx \tau_p$ is reached, the holes penetrate rather suddenly to the surface and begin to surface-compensate the electron surface traps. Now the occupation of the latter is released from the electrostatic restriction which causes the dramatic increase in the response time. Finally, $t_p$ becomes appreciably less than $\tau_p$ as $I$ is raised still further. The response time remains large and substantially constant, increasing perhaps slightly with increasing $I$ to reflect the increasing "collection efficiency" of the hole traps as the inequality $t_p < \tau_p$ becomes more pronounced.

### F. The Effect of Surface Trap Occupation on the Stability of the Surface

Yet another important consequence of the filling of the intrinsic surface states with photogenerated electrons and holes from the bulk is that the surface should be less stable under illumination than in darkness. To see why this should be, recall that the surface traps are physically the terminating lattice ions at the surface (Sec. IIE); the electron traps are the surface $Cd^{z+}$ ions and the hole traps are the surface $S^{z-}$ ions. Occupation of these traps by the appropriate carrier types alters these effective charges and so reduces their binding energies to the underlying lattice. This should manifest itself by an increase in the vapor pressure of the surface when the crystal is illuminated with greater-than-bandgap light.

This effect has recently been reported by Somorjai and Lester.[25] In a paper dealing with the effect of greater-than-bandgap illumination on the evaporation rate of insulating CdS crystals, they report that such illumination enhances the evaporation rate fivefold at 700°C and $10^{-6}$ Torr, that the rate limiting step in the evaporation is the transfer of photogenerated electrons and holes to the surface, and that the quantum efficiency for the photo-enhanced evaporation is near unity. Somorjai's interpretation of this effect, that the photogenerated electrons and holes become trapped on the surface Cd and S ions, respectively, neutralize their charges, and reduce their binding energies, is clearly consistent with the present model of intrinsic surface states.

### G. Location of the Intrinsic Surface States in the Forbidden Gap

Finally, one may estimate the location of the surface traps for electrons within the forbidden gap. The model for photo-induced chemisorption requires that the acceptor adsorbate act as a recombination center for the charge in the surface traps during the initial stages of the chemisorption process.[16] This means that the energy level of the adsorbed ions must lie below the electron trap distribution; otherwise, there would be no tendency for electrons to make transitions from the traps to the adsorbate. The energy depth of chemisorbed nitrous oxide ions is 0.74 eV [18] below the conduction band, so that a substantial fraction of the electron trap distribution must lie above this energy. An upper limit of the energy of the trap distribution can be obtained from the TSC. There is a peak in the TSC near 0°C.[16] Applying the formula for the trap depth from the location of the TSC peak,[35] which is admittedly at best only a crude estimate since this formula pertains to bulk transitions, one finds that the traps are 0.25 eV below the conduction band. Thus, the surface traps for electrons are probably distributed between 0.2 and 0.7 eV below the conduction band. This range of energies agrees with the theoretical estimates of Sec. IIE based on $z$ values lying between 0.5 and 2.

## IV. CONCLUSIONS

A comprehensive theory of surface states on ionic crystals has been derived using purely electrostatic concepts. Surface ions are considered equivalent to bulk ions except for their reduced Madelung constant. This electrostatic approach to surface states is different from the Tamm or Shockley approaches to metallic or covalent surface states. It is curious that in the history of solid-state theory, ionic crystals and electrostatic binding were considered first while metallic crystals, covalent crystals, and quantum-mechanical binding were considered second; this sequence seems to have been reversed in surface-state theory.

Energy level locations of surface states on ionic crystals are described by the dimensionless energy parameter $\epsilon$ which is calculated as a function of the surface geometry parameter $\gamma$ and the bulk material parameter $\mu$. Calculations of $\gamma$ are carried out using

[35] R. H. Bube, Ref. 29, p. 294.

surface Coulomb sums for many surface faces of NaCl, CsCl, wurtzite, and zinc-blende lattices. Calculations of $\mu$ are made for 46 ionic crystal halides, oxides, and sulfides of the form $MX$. Because the effective charge $z$ of these crystals is fractional in general, a simple procedure is used to calculate an effective $\epsilon(z)$. This flexible feature of handling fractional charges enables electrostatic principles to be applied to zinc blende and wurtzite crystals which are known to be partly ionic and partly covalent. Electrostatic criteria show that checkerboard-like surfaces are expected to be more stable than layer-like surfaces. Numerical calculations of the 48 crystals investigated show that surface states should lie closest to band center for HgS, CdS, and ZnS, and they should lie closest to the band edges for the alkali halides. Various effects can be incorporated in the above theory, if desired. They are band broadening, subsurface states, symmetry properties of the general $M_nX_m$ crystal, surface relaxations of an initially unstable $MX(L)$ surface, ion core repulsions, and the addition of partial covalency.

For the $(11\bar{2}0)$ face of CdS, detailed analysis has been made leading to an estimate of 0.2–0.4 eV for surface trap depths. Each surface $Cd^{z+}$ ion is an electron trap and each surface $S^{z-}$ ion is a hole trap.

Intrinsic surface states were detected on the $(11\bar{2}0)$ surfaces of vapor-phase-grown insulating CdS single crystal platelets with photoconductivity experiments. The intrinsic surface states were observed only when the surface was free of chemisorbed ions. The experimentally detected surface states have the following features in common with the computed intrinsic surface states: (1) The surface states function as traps for carriers from the bulk; (2) there are surface states that trap electrons as well as surface states that trap holes; (3) electrons and holes can be trapped in nearly equal numbers on an $MX(C)$-type surface; (4) the energy depth of the traps is bracketed by the limits of 0.2 and 0.7 eV. It is also shown that a large minority carrier lifetime plays a double role in the detection of the intrinsic surface states by photoconductivity measurements. First, it makes possible the isothermal desorption of chemisorbed ions that otherwise interfere with the detection of the intrinsic surface states. Second, it makes possible the surface-compensated filling of the intrinsic surface states.

PHYSICAL REVIEW VOLUME 144, NUMBER 2 15 APRIL 1966

# Mechanism of the Electrical Conduction in Li-Doped NiO

A. J. Bosman and C. Crevecoeur
*Philips Research Laboratories, N. V. Philips' Gloeilampenfabrieken, Eindhoven, Netherlands*
(Received 19 October 1965)

The electrical conductivity and the Seebeck effect are measured in the temperature region of 100 to 1300°K in NiO doped with Li. From the results it is concluded that the mobility of the charge carriers involves no activation energy. The temperature dependence of the conductivity is almost completely determined by the charge-carrier concentration. In order to calculate from the measurements the mobility $\mu$ as a function of temperature, the behavior of the density of states $N_V$ must be known. $\mu$ has been calculated for two cases, viz., $N_V$ independent of temperature and $N_V$ proportional to $T^{3/2}$. The resulting values of $\mu$ at room temperature are 0.5 and 5 $cm^2/V$ sec, respectively. In the discussion the results of Hall-effect measurements are also considered.

## I. INTRODUCTION

MANY of the transition-metal oxides, if pure and stoichiometric, are insulators. This was explained by Verwey and De Boer[1,2] by assuming the $3d$ electrons to be localized at the metal ions. According to these authors a necessary condition for an appreciable conductivity in these oxides is the presence of ions of the same element with different valency at crystallographically equivalent lattice points. In NiO this can be achieved by creating Ni vacancies or more easily by substituting Li for Ni at Ni sites. Each $Li^{1+}$ ion is then compensated by a $Ni^{3+}$ ion (principle of controlled valency[3]). At low temperatures the holes formed by the $Ni^{3+}$ are bound to the, effectively negative, $Li^{1+}$ ions. At high temperatures the holes are free and can move through the lattice by the interchange of electrons between $Ni^{3+}$ and $Ni^{2+}$ ions. It was assumed that no activation energy is needed for this process. The activation energy occurring in the conductivity must then be the energy needed for loosening the holes from the $Li^{1+}$ ions.

[1] E. J. W. Verwey and J. H. Boer, Rec. Trav. Chim. **55**, 531 (1936).
[2] J. H. de Boer and E. J. W. Verwey, Proc. Phys. Soc. (London) **49**, 59 (1937).
[3] E. J. W. Verwey, *Semiconducting Materials* (Butterworths Scientific Publications Ltd. London, 1951), pp. 151–161.